Mutual Diffusion Coefficients from NMR Imaging

Daniel Bellaire, Kerstin Münnemann, Hans Hasse*

Laboratory of Engineering Thermodynamics (LTD), TU Kaiserslautern, Germany

Abstract

In the present work, we use nuclear magnetic resonance imaging (MRI) to measure the mutual diffusion coefficient of methane in toluene at 298 K. The concentration field obtained upon dissolving gaseous methane in liquid toluene was monitored with two-dimensional MRI. To cope with the low concentration of methane, a chemical shift-selective pulse sequence was employed. The diffusion coefficient was determined from the resulting temporally and spatially resolved concentration data based on Fick's second law. The resulting diffusion coefficient is in good agreement with reference data. We conclude that MRI experiments are well-suited for quantitative studies of mutual diffusion in liquid mixtures, also in challenging applications as the one studied here.

Keywords: Mutual diffusion coefficient, NMR imaging, concentration field, methane, toluene, dissolution of gas

Introduction

Diffusion is important in many natural and technical processes. The key property for describing diffusion is the diffusion coefficient. We distinguish self-diffusion, i.e. the Brownian movement of individual particles, and mutual diffusion, i.e. the movement of particle collectives, resulting in mass transport in mixtures. Mutual diffusion is of high practical relevance, e.g. in fluid separation processes.

*Corresponding author
Email address: hans.hasse@mv.uni-kl.de (Hans Hasse)

As experimental investigations of mutual diffusion coefficients are tedious, and the number of practically relevant mixtures is extremely large, there is a lack of experimental data on this important transport property. While for gaseous mixtures, fair methods for predicting diffusion coefficients based on kinetic gas therory are available, the situation is less favorable for liquid mixtures [1, 2, 3, 4, 5, 6, 7, 8]. This is why experimental methods for the determination of mutual diffusion coefficients in liquid mixtures, as they are studied in the present work, are particularly important.

Established methods for measuring mutual diffusion coefficients in liquid mixtures include: diaphragm cells [9], wetted surface absorbers [10, 11], laminar jets [12], capillary cells [13], Taylor dispersion [14, 15], dynamic light scattering [16], and NMR techniques. In a diaphragm cell, two solutions of different composition are allowed to equilibrate through a diaphragm. The cell usually has to be calibrated with a mixture of known diffusion coefficient. In the wetted surface absorber method, a surface of defined geometry, such as a sphere or a wall, is wetted by a laminar flow and absorption into the liquid is monitored. The similar laminar jet method employs a free-flowing laminar jet in which the absorption takes place. The analysis for the two latter methods requires knowledge of the fluid dynamics for the respective geometry. In capillary cells, convective mixing is eliminated through the capillary effect: One component is placed in the capillary and then brought into contact with the second component. In the Taylor dispersion technique, a sample of a solution containing the solute and the solvent is injected into a laminar stream of the pure solvent and the dispersion of the solute after flowing through a capillary is recorded. Dynamic light scattering is able to obtain mutual diffusion coefficients from equilibrated samples. This is accomplished by observing coherent (laser) light being scattered by the sample which is influenced by local concentration fluctuations.

NMR techniques are mainly used to determine self-diffusion coefficients, in which the diffusing component is marked by a phase difference on its nuclear spin using pulsed field gradients (PFG) [17]. For infinite dilution, the self-diffusion coefficient is identical with the mutual diffusion coefficient, so that PFG-NMR

can also be used to obtain information on mutual diffusion for this state.

In the present work, we use a different NMR technique: magnetic resonance imaging (MRI). In MRI, magnetic field gradients also are applied, but in contrast to PFG-NMR, this is done in order to produce images. If the MRI images are taken component-selectively and at various times, information on the time evolution of concentration fields can be obtained, from which the mutual diffusion coefficient can be extracted. We only mention that PFG-NMR can also be used to generate spatial information in a 'diffraction-like' way [18].

With the exception of dynamic light scattering, PFG-NMR, and MRI, all of the above methods require carrying out the experiment in such a way that a special type of diffusion process is realized, which is characteristic for the method (e.g. diffusion through a diaphragm, into a laminar liquid film or jet, etc.). This is required in order to facilitate the evaluation of the experimental results, which are usually based on a time-dependent, but not spatially resolved concentration signal. Although in most cases, method-typical detectors are used for the concentration measurement, such as a refraction index detector in Taylor dispersion, the detection method with which the concentration is measured is largely exchangeable. Dynamic light scattering and PFG-NMR, on the other hand, do not require any special preparation of the diffusion process, as they can be carried out with equilibrated samples. This is not the case for MRI, which requires that macroscopic diffusion, i.e. a mass transport, occurs in the sample. However, in contrast to the other methods mentioned above, no special requirements regarding this diffusion process have to be fulfilled. Within the limits of the analytic method, any diffusion process can be monitored. In this way, MRI enables a bias-free, non-invasive, and direct observation of diffusion processes.

In previous work, MRI has been applied to acquire one-dimensional (1D) diffusion profiles of water in polymers [19, 20, 21] and solvents in porous materials [22]. 2D imaging studies have been carried out to study the diffusion of different solvents in polymers [23, 24, 25, 26] and of water in solids such as catalyst pellets [27], clay [28], or asphalt [29]. If required, MRI is also able to

provide 3D resolution, as demonstrated in a study of microstructure growth in battery cells [30]. Most of theses studies were carried out with ^{1}H NMR. MRI studies of diffusion employing other nuclei have been reported for ^{23}Na [31], ^{31}P [32], or ^{19}F and ^{7}Li [33]. Through indirect detection, e.g. by observing variations of T_1 or T_2 relaxation times in the sample, even species, such as radicals, that are difficult to detect otherwise, can be tracked [34]. The above mentioned studies investigate diffusion into immobilized materials such as polymers or solids. Measuring diffusion in liquids poses greater difficulties. This is due to the occurrence of convection.

1D MRI has been used for the purpose of measuring the diffusion of carbon dioxide in an ionic liquid [35] and for measuring the diffusion in a triethylamine/water system [36, 37]. Here, we employ 2D MRI to study the diffusion of a dissolved gas, methane, in a liquid, toluene. This is particularly challenging due to the low concentrations of the solute.

In most of the mentioned literature studies, a gradient echo [38] or a spin-echo [39] pulse sequence was used.

There is, furthermore, much literature on a technique known as diffusion-weighted imaging (DWI), which is only related to the topic of the present work, as it uses the physical effect of diffusion to enhance the contrast in MR imaging, mainly in medical applications [40, 41, 42, 43].

The present study was carried out as a part of a large project on mass transfer through fluid interfaces, in which we were particularly interested in mass transfer at vapor-liquid interfaces in systems that show a high enrichment of the transferred component at the interface. This is the case for the system (methane + toluene) studied in the present work, for which an enrichment of about 2.5 is predicted for the conditions studied here with the method proposed in [44]. Herein, the enrichment is the ratio of the highest molar density of methane in the interfacial region to the higher of the two molar densities in the bulk phases, which is the gas phase here. Furthermore, we have recently determined mutual diffusion coefficients at infinite dilution from an extrapolation of self-diffusion coefficient data from PFG-NMR and obtained also results for the

system (methane + toluene) [45]. In the experiments carried out in the present study, we have monitored the loading of liquid toluene with methane from a gas phase at a moderate pressure, resulting in sufficiently low concentrations of methane in the liquid to allow a direct comparison of the resulting mutual diffusion coefficient with that for infinite dilution obtained from the PFG-NMR data in the previous study [45].

To cope with the fact that the methane signals are much weaker than the toluene signals, due to the low methane concentration, a chemical shift-selective RARE (Rapid Acquisition with Relaxation Enhancement) [46, 47] pulse sequence was used. With that pulse, sequence 2D images of methane diffusing into toluene were collected. The chemical shift-selectivity enables the observation of methane without the interference from the strong toluene background signal.

From the MRI results, quantitative information on the concentration field of methane in the liquid was obtained. A model based on Fick's second law was applied to extract the information on the mutual diffusion coefficient from that data. Fick's second law can be applied here due to the low methane concentration.

At the conditions studied here, the mutual diffusion coefficients according to Fick and Maxwell-Stefan and the self-diffusion coefficient of methane in toluene are practically identical, so that we will use the term diffusion coefficient for simplicity in the following. The paper is divided into an experimental section reporting on the sample preparation and the MRI method. Then, the theory applied for the data analysis is described. This is followed by the results section in which the experimental data and their interpretation are presented and discussed.

Experiments

^{1}H NMR spectra and images were recorded with a Bruker Biospin NMR spectrometer with a magnetic field strength of 7.05 T, corresponding to a pro-

ton Larmor frequency of 300.13 MHz, equipped with a microimaging probe with a quadrature detection resonator (magnet: Ascend 300 wide bore; console: Avance Neo). The acquisition software was `Paravision 360` (version 1.1, Bruker BioSpin MRI GmbH). The spectrometer's temperature control unit was calibrated with a platinum resistance thermometer (Pt-100) which was, in turn, calibrated using a standard, certified by PTB, Braunschweig. The standard uncertainty of the temperature measurement is estimated to be $u(T) = 0.2$ K. The measurements were carried out in a pressure-tight glass sample tube (FengTecEx GmbH, P16, 38 ml, inner diameter 19 mm) which is depicted in Fig. 1. The cap of the sample tube was designed in the present work. It seals the tube and enables its connection to the gas feed line and ensures a favorable distribution of the gas in the tube.

The sample cell was filled with toluene such as to match the following criteria: First, the top of the measurement region should be at least 10 mm below the gas-liquid interface (but not much more) so that measurement problems resulting from inhomogeneities of the magnetic field are avoided. The distance between the interface and the upper end of the measurement region is denoted with z_0 here. Second, the tube should be filled with as much toluene as possible, while still fitting into the resonator and fulfilling the first criterion. This ensures that there is enough toluene in the volume below the measurement region to justify the assumption of the semi-infinite medium [48] which is used in the analysis.

The toluene that was used in this work was obtained from AppliChem GmbH (CAS 108-88-3, purity 0.999 mol·mol^{-1}). The methane gas was obtained from Air Liquide S.A. (CAS 74-82-8, purity 0.99 mol·mol^{-1}). The chemicals were used without further purification.

For a simple evaluation of the results, it is essential to avoid convection. Convection could be induced by the gas flow into the cell which is, however, very low during the experiments. Furthermore, free convection could be induced by density gradients driven by concentration gradients. This can be excluded as the methane is fed from the top and its dissolution in the toluene leads to a lower density. Furthermore, the corresponding density change is very small, as

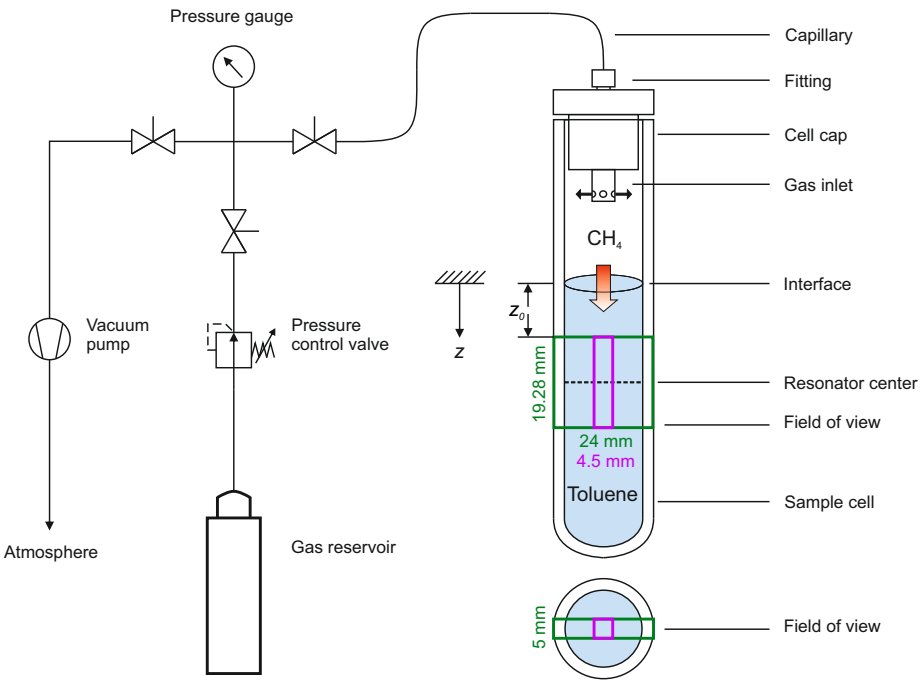

Figure 1: Experimental setup that was used for the imaging experiments. The measurement volume (green) and the volume used for the analysis (magenta) are indicated.

the methane concentration is very low at all times. Last but not least, natural convection could be caused by temperature gradients in the cell. As the equilibration time was very long in the present experiments, temperature gradients could only be caused by deficiencies of the thermostatting system. This cannot be excluded a priori, as has been pointed out by Barbosa et al. [49]. These authors found that the corresponding problems depend on the temperature of the instrument and are expected to be smallest near room temperature, which is where we have carried out our experiments.

Furthermore, as we have 2D information on the penetration of the gas into the liquid, we can detect a possible influence of convection. At the conditions that are of interest here, any convective flow pattern in the cell must be laminar and circular, with low velocities near the wall due to the no-slip condition. It follows from the mass balance that, if the convection is downward near the axis,

there must be a zone between the axis and the wall where the convection is upward (and vice versa). Downward convection accelerates the penetration of the gas into the liquid, upward convection slows it down. In any case, near the wall, where there is no convection, the penetration is only caused by diffusion and correct results would be expected. Hence, if convection would have occurred, it should have led to characteristic distortions of the observed concentration profiles, which should have been detectable in the 2D MRI experiments. The patterns we have observed, see Supplementary Information, give no indication of the presence of convection. This is further supported by the fact that the result we have obtained for the diffusion coefficient (without any calibration) is in excellent agreement with literature data. A more detailed discussion of the issue of convection is given in the Supplementary Material.

In this work, the RARE pulse sequence [46] was extended in order to be chemical shift-selective (courtesy of Bruker Biospin) and is depicted in Fig. 2. The RARE sequence is very similar to the MSME (Multi Slice Multi Echo) sequence [39]. In MSME, as in RARE, images of one or more slices are generated by recording a CPMG [50, 51] echo train. The length of the echo train, i.e. the number of generated echos, is determined by the number of repeated refocusing steps which is represented by the bracketed part of the pulse sequence in Fig. 2. Spatial resolution is achieved by frequency- and phase-encoding each echo. In the MSME sequence, each echo experiences the same phase-encoding and the successive echos can be used to improve the signal-to-noise ratio (SNR) or for T_2 relaxation experiments. In the RARE sequence, each echo is individually phase-encoded and therefore represents different lines in k-space instead of the same one as is the case for MSME. This enables a much faster image acquisition, by a factor of R, the so-called RARE factor which determines the number of phase-encoded echos obtained from one echo train, cf. Fig. 2.

The 90° excitation pulse at the beginning of the pulse sequence is made chemical shift-selective in order to be able to observe the signal originating from methane without the large background solvent signal stemming from toluene that would otherwise be present. The NMR parameters for the selective ex-

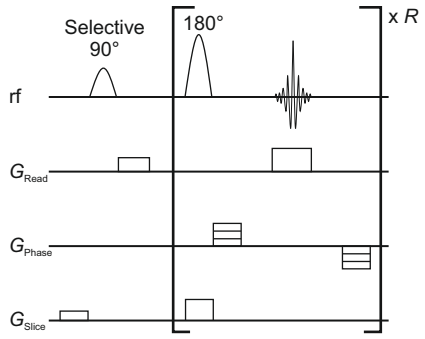

Figure 2: Chemical shift-selective RARE sequence that was used for the imaging experiments. The part in brackets is repeated R times with R being the RARE factor. The total duration of the pulse sequence is 503 ms with $R = 32$.

citation of methane were determined beforehand using an equilibrated sample containing toluene and methane. For the chemical shift-selective excitation pulse, a Gaussian shape and a bandwidth of 200 Hz were found to be optimal. The bottom of Fig. 3 shows the ^{1}H NMR spectrum after selective excitation of the methane peak at 2.8 ppm. The non-selectively excited ^{1}H NMR spectrum is shown at the top in Fig. 3 for comparison. It can be seen that although the methane peak is cleanly excited, a small residue of the neighboring toluene peak remains visible. This residue is compensated during the measurement process, see below.

The experiment was carried out as follows: The sample cell was filled with toluene as described above, closed with its cap, and inserted into the resonator. The resonator with the sample cell was then mounted in the NMR probe and placed in the magnet. The capillary was then connected to the pressure control unit and the gas reservoir. Before the gas application was started, a background image was recorded, which was later subtracted from the obtained images. This eliminated any residual signal from the toluene in the images due to slightly imperfect selective excitation of the methane, cf. Fig. 3. Furthermore, a reference image using pure toluene was collected and the toluene signal was used for normalizing the slightly inhomogeneous excitation of the sample region. A

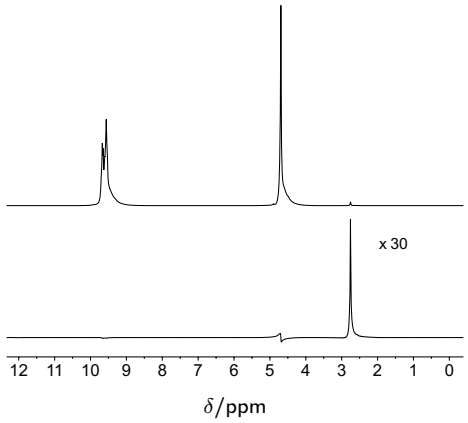

Figure 3: ^{1}H NMR spectra of the system (methane + toluene). The toluene was saturated with methane at 0.4 MPa and 298.15 K. The upper spectrum is a standard spectrum and shows only a very small signal of the protons in methane. The bottom spectrum (magnified) was recorded after selective excitation of the methane peak at about 2.8 ppm.

map of the radio frequency (RF) field homogeneity of the resonator is shown in the Supplementary Material. In the next step, the sample cell was connected to the vacuum pump, by opening a valve. The valve was opened only about a second, which is sufficient to remove the air from the sample cell. Then, the cell was connected to the methane cylinder and the pressure was adjusted to 0.4 MPa using a pressure gauge (WIKA P-30). Together with the pressurization, the pulse sequence was started. Every 16 minutes, an image was produced which consisted of an average of 32 individual images from these 16 minutes. In this way, 240 (averaged) images were recorded during the overall duration of the experiment of 64 hours. The process of averaging over 16 minutes introduces a certain blur in the measured time variable, which is, however, negligible considering the overall duration of the diffusion process.

The parameter values that were used for the imaging experiment are listed in Table 1.

From the sample, a slice of 5 mm thickness (in x-direction in Fig. 1) was excited. The slice thickness of 5 mm was chosen since this value produces a sufficiently high intensity signal while still exciting an almost cuboid part of the

Table 1: Parameters for the chemical shift-selective RARE pulse sequence that was used for the imaging experiments.

Pulse sequence parameters	
Excitation pulse bandwidth	200 Hz
Excitation pulse shape	Gauss
Excitation pulse length	13.7 ms
Refocusing pulse bandwidth	4200 Hz
Refocusing pulse length	0.8 ms
Slice thickness	5.00 mm
Field of view	19.28 x 24.00 (z x y) mm
Image size	56 x 32 (z x y) pixels
Echo spacing	15.3 ms
Repetition time	30 s
RARE factor	32
Averages per Image	32

sample. From this slice, a measurement region (field of view), which is depicted as a green rectangle in Fig. 1, was chosen in such a way that it covers the region inside the resonator which experiences the most homogeneous excitation. The homogeneity of the excitation was determined beforehand through an RF excitation field map of the resonator. The usable field of view spans an area of 19.28 x 24.00 mm in z- and y-direction. It is subdivided into a Cartesian pixel grid of 56 x 32 (z x y). This results in volume elements (voxels) of about 1.3 mm^3. The voxel dimensions (and therefore the spatial resolution of the experiment) are 5.00 x 0.34 x 0.75 mm in the x-, z-, and y-directions, respectively. With these settings, the three outermost voxels on each side are positioned inside the glass wall of the sample cell and are serving as 'baseline' voxels, i.e. giving a constant zero signal to which the rest of the data can be compared. Of the remaining voxels, only the respective outermost on each side of the image lie in the curvature of the round sample cell. All other voxels occupy the same

volume of sample material and have therefore equivalent spin density. For each voxel, a scalar intensity value is obtained selectively from all methane protons in the voxel through integration of the respective echo signal. This produces a 2D image at each time step t and t is taken in the middle of the 16 minute interval used for the acquisition.

The repetition time of 30 s allows for a sufficient relaxation of the sample spins before the next excitation. Due to methane having a large T_2 relaxation time constant of 6 s ($U(T_2) = 0.2\ s$ with a coverage factor of $k = 2$), a rather large RARE factor of 32 can be chosen. This means that with each excitation and therefore each CPMG echo train, a whole 2D image is recorded. From 32 individual images, one average image with improved SNR is constructed. As mentioned above, this still introduces a T_2 weighting into the images. However, this only affects the y-direction, it has no influence on the diffusion analysis.

Model-based Data Analysis

Although 2D images of the diffusion process were recorded, the evaluation is carried out here based on a 1D diffusion model. This is facilitated by an appropriate choice of the voxels that are used for the evaluation, as explained below in more detail. The spatial coordinate used here (z) coincides with the symmetry axis of the cylindrical sample cell geometry. The diffusion along the z axis is analyzed using Fick's second law, Eq. (1). [52]

$$\frac{\partial c_1(z,t)}{\partial t} = D_{12} \frac{\partial^2 c_1(z,t)}{\partial z^2} \tag{1}$$

c_1 is the molarity of methane, t is the time, and D_{12} is the constant mutual diffusion coefficient of methane (1) in toluene (2).

In this work, the solution of Eq. (1) for a semi-infinite medium with a concentration jump at the boundary at $t = 0$ is used [48] which is given by Eq. (2).

$$c_1(z,t) = c_{1,0}\ \mathrm{erfc}\left(\frac{z}{2\sqrt{D_{12}t}}\right) \tag{2}$$

where $c_{1,0}$ stands for a constant concentration at the boundary, i.e. the gas-liquid interface, and erfc() denotes the complementary Gaussian error function. This solution holds for the following boundary and initial conditions, Eq. (3) and Eq. (4), respectively.

$$c_1 = c_{1,0}, \quad z = 0, \quad t > 0 \tag{3}$$

$$c_1 = 0, \quad z > 0, \quad t = 0 \tag{4}$$

The origin of the z axis is at the interface with increasing z values downwards in the liquid phase, cf. Fig. 1. It can be assumed that toluene is saturated with methane at the interface, hence $c_{1,0} = c_{1,\mathrm{sat}}$. The value $c_{1,\mathrm{sat}}$ for the conditions studied in the present work is available from our previous work [45] and is found to be $c_{1,\mathrm{sat}} = 0.047$ mol·dm^{-3} (abs. uncertainty $u(c_{1,\mathrm{sat}}) = 0.005$ mol·dm^{-3}; using the density of pure toluene [53] for the conversion of mole fraction to molarity).

Since the concentration is proportional to the measured intensity per voxel, I, Eq. (5) holds.

$$\frac{I(z,t)}{I_0} = \frac{c_1(z,t)}{c_{1,0}} = \mathrm{erfc}\left(\frac{z}{2\sqrt{D_{12}t}}\right) \tag{5}$$

Here, I_0 is the constant intensity which would be measured at the gas-liquid interface equivalent to the constant concentration at that location $c_{1,0}$. As the field of view is shifted downwards from the surface by z_0, cf. Fig. 1, a coordinate z^*, which originates at the top of the field of view, is defined as follows:

$$z^* = z - z_0 \tag{6}$$

Using Eq. (5), D_{12}, I_0, and z_0 were obtained from a fit of Eq. (2) to the experimental data. As the diffusion process is assumed to be one-dimensional in z, results for the same z but different y are averaged before the fitting procedure. The model was implemented in Matlab (version R2019a). The model parameters

D_{12}, I_0, and z_0 were determined from a least squares fit using the Matlab function `fit` which is based on a trust-region algorithm.

Results and Discussion

Fig. 4 shows 2D images of the diffusion process of methane in toluene. The presented images correspond to the volume indicated in magenta color in Fig. 1. The image data of the complete field of view (green in Fig. 1) are shown in the Supplementary Material. Only the six vertical voxel columns in the center of the field of view (around the sample tube's axis) were chosen for the evaluation and the corresponding image data are shown in Fig. 4. There are several reasons for restricting the volume used for the quantification: 1) The curvature of the surface can be neglected, which facilitates the evaluation; 2) wall effects play no role; 3) the homogeneity of the RF excitation field is best near the axis. A more detailed discussion of these effects is given in the Supplementary Material.

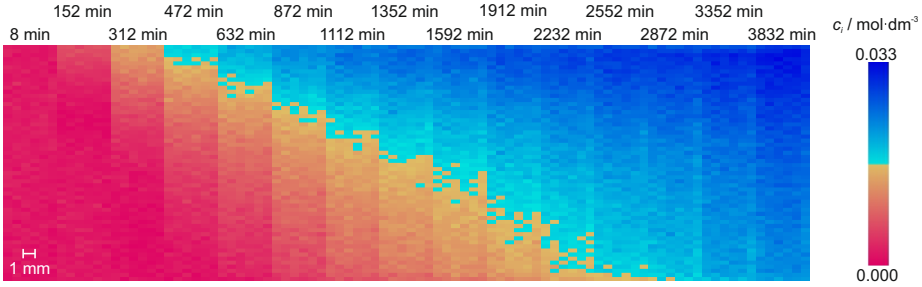

Figure 4: 2D images of the methane molarity c_1 for different times during the diffusion experiment. The color codes represent the concentration of the selectively excited methane, which diffuses downwards into the toluene.

In Fig. 4, only 18 images, out of the 240 images that were measured in total, taken at different times during the experiment are presented. To obtain a meaningful scaling, the intensity data of the image data was converted to data on the methane molarity c_1 using Eq. (5); the saturation value $c_{1,0}$ was adopted from the literature [45] and is $c_{1,\mathrm{sat}} = 0.047$ mol·dm^{-3} (abs. uncertainty $u(c_{1,\mathrm{sat}}) = 0.005$ mol·dm^{-3}). Despite the low solubility of methane in toluene

and therefore low signal intensity, the images have a good signal-to-noise ratio (SNR). Methane can be seen diffusing downwards into the toluene until the field of view is almost saturated. For a given value of z, the results from the six voxels in y direction were simply averaged to obtain a signal I that only depends on the position z and the time t.

That signal was evaluated using Eq. (5). Thereby, the number of the diffusion coefficient D_{12} was obtained from a fit to the data as described above. Besides the diffusion coefficient D_{12} also the height z_0 as well as the intensity I_0 were determined from the fit. The number z_0 is hard to determine geometrically with sufficient accuracy due to the curvature. The number of I_0 could have been determined alternatively from a measurement of the saturated solution, which would have been more complicated without promising any advantage. The result of the fit is shown in Fig. 5, the numerical results for D_{12}, z_0 and I_0 are given in Table 2.

The plot in Fig. 5 shows the results for $c_1/c_{1,0}$ as a function of t and $z^* = z - z_0$. Experimental data are shown as points, the fit as a surface.

Table 2: Result of the fit of Eq. (2) to the experimental data. The expanded, last digit uncertainties ($k = 2$) are given in parentheses.

	Fit result
D_{12}	$5.24(10)\cdot10^{-9}$ m^2·s^{-1}
z_0	15.1(3) mm
I_0	1.42(1) a.u.

As shown in Fig. 5, the fitted surface describes the experimental data generally well which is also reflected by the R^2 value of the fit, which is 0.98. Systematic deviations are observed basically only in the upper left corner of the diagram, i.e. for large times at the upper end of the measuring window. This could be the result of an increasing influence of the curved interface. This hypothesis could be checked by numerical simulations, which were, however, not in the scope of the present work. As mentioned before, the equilibrium concentration

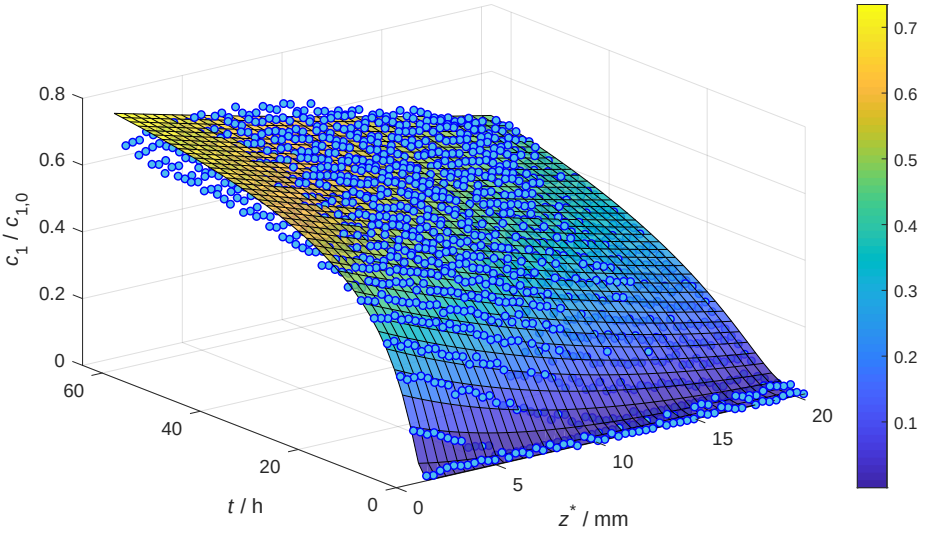

Figure 5: Relative molarity of methane as a function of time and position. The reference $c_{1,0}$ is the saturation value. Experimental values (blue dots) are compared to results from the model fit (surface), from which the number of the diffusion coefficient was obtained. For clarity, only every tenth experimental data point is shown.

of methane in toluene is only about 0.5 mol-% for the studied conditions. Therefore, the range of compositions in the studied diffusion process is small so that it can be assumed that the corresponding mutual diffusion coefficient is constant. Furthermore, it can be assumed that the mutual diffusion coefficient is equal to that at infinite dilution of methane which allows the comparison with published literature data. The diffusion coefficient of methane in toluene at 298 K has been measured recently by PFG-NMR [45] and found to be $D_{12} = 5.32 \cdot 10^{-9}$ m^2·s^{-1} (expanded uncertainty $U(D_{12}) = 0.27 \cdot 10^{-9}$ m^2·s^{-1} ($k = 2$)). This value and the one found in the present study agree within their respective uncertainties. This is a strong argument for the applicability of the MRI method presented here for studying mutual diffusion coefficients and it also supports the chosen way of the data evaluation. Furthermore, also the value found for z_0 agrees well with the distance between the interface and the top of the field of view.

Conclusions

In this work, the dissolution of methane from a gas phase at 0.4 MPa in liquid toluene was monitored by MRI at 298 K. A chemical shift-selective RARE pulse sequence was applied in order to selectively record concentration field images of the highly diluted methane at consecutive time steps. The diffusion coefficient of methane in toluene was determined from the data based on Fick's second law and was found to be in excellent agreement with literature data. Two-dimensional imaging was applied and using the results from voxels near the symmetry axis of the sample tube, data on a one-dimensional time-dependent methane concentration field were obtained. These data were analyzed with the well-known solution of Fick's second law for a semi-infinite slab with a concentration jump on the surface, which gave the good results mentioned above. There are several reasons for restricting the volume used for the quantification: the curvature of the surface can be neglected, which facilitates the evaluation; wall effects play no role; the homogeneity of the RF excitation field is best near the axis.

Although measuring diffusion by MRI requires suitable NMR equipment, the experiments themselves are relatively simple. In our case, a pressurized sample tube was sufficient. Challenges arise, however, from the necessity to avoid natural convection, which can in principle be driven by concentration or temperature gradients. Both effects did not play a role in the present experiments, as can be inferred from the 2D MRI data that was taken.

The information on the diffusion coefficient has to be extracted from the MRI data by a model-based quantitative evaluation. In the present work, a simple straightforward approach was used for this, which consisted basically in using only those parts of the data, to which an available analytical solution could be applied.

We have demonstrated here, that quantitative studies of mutual diffusion with MRI techniques are feasible also in challenging situations, such as low concentrations of diffusing solutes. For obtaining diffusion coefficients of diluted

gases in liquids, also PFG-NMR can be used, which is a simpler technique. However, PFG-NMR yields only information on self-diffusion, which only coincides with mutual diffusion for the case of infinite dilution. In contrast, MRI can be applied for studies of mutual diffusion at any concentration, which is highly relevant for technical applications. Furthermore, we have applied MRI here only to study diffusion in a simple binary liquid mixture. The technique, however, lends itself also to study diffusion in more complex situations: profiting from the high chemical shift dispersion, also multicomponent diffusion and diffusion in reactive systems can be studied, and MRI is also suited to study diffusion in geometrically confined spaces, such as packed beds. The evaluation of the MRI results is facilitated if there is no convection, but even in the presence of convection, it should in principle be possible to obtain meaningful results, as concentration fields of all components can be measured for any point in time. The strength of the method is that it is non-invasive and can be applied directly to the system under scrutiny, as long as it fits into the bore of the MRI magnet. Wide-bore NMR magnets are therefore desirable. However, the present study also shows that there are substantial challenges namely those related to the quantification, which requires excellent field homogeneity in the studied volume. Studying diffusion of highly diluted components is possible, however, at the cost of the time resolution, which was of the order of 10 min for a diffusion process that took about 100 h in the present study, but the settings can be adapted to study also faster processes.

MRI is an excellent and flexible tool for quantitative studies of mutual diffusion, and offers many opportunities, which we are only beginning to exploit.

Acknowledgments

This project has received funding from the European Research Council (ERC) under the European Union's Horizon 2020 research and innovation program under grant agreement No. 694807 ENRICO. The authors thank Thomas Oerther (Bruker Biospin) for help with the adaptation of the pulse sequence

which was used in this work.

References

[1] L. S. Darken, Diffusion, mobility and their interrelation through free energy in binary metallic systems, Trans. Am. Inst. Min. Metall. Eng. 175 (1948) 184–201.

[2] A. Vignes, Diffusion in binary solutions: Variation of diffusion coefficient with composition, Ind. Eng. Chem. Fund. 5 (2) (1966) 189–199.

[3] C. R. Wilke, P. Chang, Correlation of diffusion coefficients in dilute solutions, AIChE J. 1 (2) (1955) 264–270. doi:10.1002/aic.690010222.

[4] R. Evans, G. Dal Poggetto, M. Nilsson, G. A. Morris, Improving the interpretation of small molecule diffusion coefficients, Anal. Chem. 90 (6) (2018) 3987–3994. doi:10.1021/acs.analchem.7b05032.

[5] M. T. Tyn, W. F. Calus, Diffusion coefficients in dilute binary liquid mixtures, J. Chem. Eng. Data 20 (1) (1975) 106–109. doi:10.1021/je60064a006.

[6] W. Hayduk, B. S. Minhas, Correlations for prediction of molecular diffusivities in liquids, Can. J. Chem. Eng. 60 (2) (1982) 295–299. doi:10.1002/cjce.5450600213.

[7] K. Nakanishi, Prediction of diffusion coefficient of nonelectrolytes in dilute solution based on generalized Hammond-Stokes plot, Ind. Eng. Chem. Fund. 17 (4) (1978) 253–256. doi:10.1021/i160068a004.

[8] K. A. Reddy, L. K. Doraiswamy, Estimating liquid diffusivity, Ind. Eng. Chem. Fund. 6 (1) (1967) 77–79. doi:10.1021/i160021a012.

[9] M. J. Tham, K. K. Bhatia, K. F. Gubbins, Steady-state method for studying diffusion of gases in liquids, Chem. Eng. Sci. 22 (3) (1967) 309–311. doi:10.1016/0009-2509(67)80117-9.

[10] A. Tamimi, E. B. Rinker, O. C. Sandall, Diffusion coefficients for hydrogen sulfide, carbon dioxide, and nitrous oxide in water over the temperature range 293-368 K, J. Chem. Eng. Data 39 (2) (1994) 330–332. doi:10.1021/je00014a031.

[11] S. Lee, H.-J. Song, S. Maken, H.-C. Shin, H.-C. Song, J.-W. Park, Physical solubility and diffusivity of N2O and CO2 in aqueous sodium glycinate solutions, J. Chem. Eng. Data 51 (2) (2006) 504–509. doi:10.1021/je0503913.

[12] J. M. Diaz, A. Vega, J. Coca, Diffusivities of carbon dioxide and nitrous oxide in aqueous alcohol solutions, J. Chem. Eng. Data 33 (1) (1988) 10–12. doi:10.1021/je00051a004.

[13] V. K. Malik, W. Hayduk, A steady-state capillary cell method for measuring gas-liquid diffusion coefficients, Can. J. Chem. Eng. 46 (6) (1968) 462–466. doi:10.1002/cjce.5450460614.

[14] G. I. Taylor, Dispersion of soluble matter in solvent flowing slowly through a tube, Proc. R. Soc. A 219 (1137) (1953) 186–203. doi:10.1098/rspa.1953.0139.

[15] R. Aris, On the dispersion of a solute in a fluid flowing through a tube, Proc. R. Soc. A 235 (1200) (1956) 67–77. doi:10.1098/rspa.1956.0065.

[16] R. D. Mountain, J. M. Deutch, Light scattering from binary solutions, J. Chem. Phys. 50 (3) (1969) 1103–1108. doi:10.1063/1.1671163.

[17] D. Bellaire, H. Kiepfer, K. Münnemann, H. Hasse, PFG-NMR and MD simulation study of self-diffusion coefficients of binary and ternary mixtures containing cyclohexane, ethanol, acetone, and toluene, J. Chem. Eng. Data 65 (2) (2020) 793–803. doi:10.1021/acs.jced.9b01016.

[18] P. T. Callaghan, A. Coy, D. MacGowan, K. J. Packer, F. O. Zelaya, Diffraction-like effects in NMR diffusion studies of fluids in porous solids, Nature 351 (6326) (1991) 467–469. doi:10.1038/351467a0.

[19] P. Y. Ghi, D. J. T. Hill, D. Maillet, A. K. Whittaker, N.m.r. imaging of the diffusion of water into poly(tetrahydrofurfuryl methacrylate-co-hydroxyethyl methacrylate), Polymer 38 (15) (1997) 3985–3989. doi:10.1016/S0032-3861(96)01071-3.

[20] T. M. Hyde, L. F. Gladden, Simultaneous measurement of water and polymer concentration profiles during swelling of poly(ethylene oxide) using magnetic resonance imaging, Polymer 39 (4) (1998) 811–819. doi:10.1016/S0032-3861(97)00328-5.

[21] S. Blackband, P. Mansfield, Diffusion in liquid-solid systems by NMR imaging, J. Phys. C: Solid State Phys. 19 (2) (1986) L49–L52. doi:10.1088/0022-3719/19/2/004.

[22] N.-K. Bär, B. J. Balcom, D. M. Ruthven, Direct measurement of transient concentration profiles in adsorbent particles and chromatographic columns by MRI, Ind. Eng. Chem. Res. 41 (9) (2002) 2320–2329. doi:10.1021/ie010821s.

[23] S. Baumgartner, G. Lahajnar, A. Sepe, J. Kristl, Quantitative evaluation of polymer concentration profile during swelling of hydrophilic matrix tablets using 1H NMR and MRI methods, Eur. J. Pharm. Biopharm. 59 (2) (2005) 299–306. doi:10.1016/j.ejpb.2004.08.010.

[24] L. A. Weisenberger, J. L. Koenig, NMR imaging of diffusion processes in polymers: measurement of the spatial dependence of solvent mobility in partially swollen PMMA rods, Macromolecules 23 (9) (1990) 2445–2453. doi:10.1021/ma00211a007.

[25] R. A. Grinsted, J. L. Koenig, Study of multicomponent diffusion into polycarbonate rods using NMR imaging, Macromolecules 25 (4) (1992) 1229–1234. doi:10.1021/ma00030a005.

[26] K. P. Nott, Magnetic resonance imaging of tablet dissolution, Eur. J.

Pharm. Biopharm. 74 (1) (2010) 78–83. doi:10.1016/j.ejpb.2009.07.003.

[27] M. Hollewand, L. Gladden, Heterogeneities in structure and diffusion within porous catalyst support pellets observed by NMR imaging, J. Catal. 144 (1) (1993) 254–272. doi:10.1006/jcat.1993.1328.

[28] S. V. Dvinskikh, K. Szutkowski, I. Furó, MRI profiles over very wide concentration ranges: Application to swelling of a bentonite clay, J. Magn. Reson. 198 (2) (2009) 146–150. doi:10.1016/j.jmr.2009.01.035.

[29] F. P. Miknis, A. T. Pauli, A. Beemer, B. Wilde, Use of NMR imaging to measure interfacial properties of asphalts, Fuel 84 (9) (2005) 1041–1051. doi:10.1016/j.fuel.2004.12.019.

[30] A. J. Ilott, M. Mohammadi, H. J. Chang, C. P. Grey, A. Jerschow, Real-time 3D imaging of microstructure growth in battery cells using indirect MRI, Proc. Natl. Acad. Sci. U.S.A. 113 (39) (2016) 10779–10784. doi:10.1073/pnas.1607903113.

[31] C. Vestergaard, J. Risum, J. Adler-Nissen, 23Na-MRI quantification of sodium and water mobility in pork during brine curing, Meat Science 69 (4) (2005) 663–672. doi:10.1016/j.meatsci.2004.11.001.

[32] S. Kwak, M. T. P. Viet, M. Lafleur, Self- and mutual-diffusion coefficients measurements by 31P NMR 1D profiling and PFG-SE in dextran gels, J. Magn. Reson. 162 (1) (2003) 198–205. doi:10.1016/S1090-7807(03)00047-8.

[33] M. Ditter, M. Becher, S. Orth, K. Schwartz, C. Trautmann, F. Fujara, Spatially resolved magnetic resonance studies of swift heavy ion induced defects and radiolysis products in LiF crystals, Nuclear Inst. and Methods in Physics Research B 441 (2019) 70–78. doi:10.1016/j.nimb.2018.11.040.

[34] B. J. Balcom, A. E. Fischer, T. A. Carpenter, L. D. Hall, Diffusion in aqueous gels. Mutual diffusion coefficients measured by one-dimensional nuclear magnetic resonance imaging, J. Am. Chem. Soc. 115 (8) (1993) 3300–3305. doi:10.1021/ja00061a031.

[35] J. Allen, K. Damodaran, High-resolution slice selection NMR for the measurement of CO2 diffusion under non-equilibrium conditions, Magn. Reson. Chem. 53 (3) (2015) 200–202. doi:10.1002/mrc.4176.

[36] C. F. Pantoja, J. A. Bolaños, A. Bernal, J. Wist, Mutual diffusion driven NMR: a new approach for the analysis of mixtures by spatially resolved NMR spectroscopy, Magn. Reson. Chem. 55 (6) (2017) 519–524. doi:10.1002/mrc.4561.

[37] C. F. Pantoja, Y. M. Muñoz-Muñoz, L. Guastar, J. Vrabec, J. Wist, Composition dependent transport diffusion in non-ideal mixtures from spatially resolved nuclear magnetic resonance spectroscopy, Phys. Chem. Chem. Phys. 20 (44) (2018) 28185–28192. doi:10.1039/C8CP05539D.
URL http://xlink.rsc.org/?DOI=C8CP05539D

[38] A. Haase, J. Frahm, D. Matthaei, W. Hänicke, K.-D. Merboldt, FLASH imaging. Rapid NMR imaging using low flip-angle pulses, J. Magn. Reson. 67 (2) (1986) 258–266. doi:10.1016/0022-2364(86)90433-6.

[39] D. A. Feinberg, C. M. Mills, J. P. Posin, D. A. Ortendahl, N. M. Hylton, L. E. Crooks, J. C. Watts, L. Kaufman, M. Arakawa, J. C. Hoenninger, M. Brant-Zawadzski, Multiple spin-echo magnetic resonance imaging, Radiology 155 (2) (1985) 437–442. doi:10.1148/radiology.155.2.3983396.

[40] R. Bammer, Basic principles of diffusion-weighted imaging, Eur. J. Radiol. 45 (3) (2003) 169–184. doi:10.1016/S0720-048X(02)00303-0.

[41] V. Baliyan, C. J. Das, R. Sharma, A. K. Gupta, Diffusion weighted imaging: Technique and applications, World J. Radiol. 8 (9) (2016) 785–798. doi:10.4329/wjr.v8.i9.785.

[42] P. Hagmann, L. Jonasson, P. Maeder, J.-P. Thiran, V. J. Wedeen, R. Meuli, Understanding diffusion MR imaging techniques: From scalar diffusion-weighted imaging to diffusion tensor imaging and beyond, RadioGraphics 26 (suppl_1) (2006) S205–S223. doi:10.1148/rg.26si065510.

[43] A. Gupta, T. Stait-Gardner, W. S. Price, NMR imaging and diffusion, Adsorption 27 (3) (2021) 503–533. doi:10.1007/s10450-021-00298-9.

[44] S. Stephan, H. Hasse, Enrichment at vapour–liquid interfaces of mixtures: Establishing a link between nanoscopic and macroscopic properties, Int. Rev. Phys. Chem. 39 (3) (2020) 319–349. doi:10.1080/0144235X.2020.1777705.

[45] D. Bellaire, O. Großmann, K. Münnemann, H. Hasse, Diffusion coefficients at infinite dilution of carbon dioxide and methane in water, ethanol, cyclohexane, toluene, methanol, and acetone: A PFG-NMR and MD simulation study, J. Chem. Thermodyn. 166 (2022) 106691. doi:10.1016/j.jct.2021.106691.

[46] J. Hennig, A. Nauerth, H. Friedburg, RARE imaging: A fast imaging method for clinical MR, Magn. Reson. Med. 3 (6) (1986) 823–833. doi:10.1002/mrm.1910030602.

[47] J. Kind, C. Thiele, MRI and localised NMR spectroscopy of sessile droplets on hydrophilic, hydrophobic and superhydrophobic surfaces – Examination of the chemical composition during evaporation, J. Magn. Reson. 307 (2019) 106579. doi:10.1016/j.jmr.2019.106579.

[48] J. Crank, The mathematics of diffusion, 2nd Edition, Clarendon Press, Oxford, 1975.

[49] T. M. Barbosa, R. Rittner, C. F. Tormena, G. A. Morris, M. Nilsson, Convection in liquid-state NMR: expect the unexpected, RSC Adv. 6 (97) (2016) 95173–95176. doi:10.1039/C6RA23427E.

[50] H. Y. Carr, E. M. Purcell, Effects of diffusion on free precession in nuclear magnetic resonance experiments, Phys. Rev. 94 (3) (1954) 630–638. doi:10.1103/PhysRev.94.630.

[51] S. Meiboom, D. Gill, Modified spin-echo method for measuring nuclear relaxation times, Rev. Sci. Instrum. 29 (8) (1958) 688–691. doi:10.1063/1.1716296.

[52] A. Fick, Über Diffusion, Ann. Phys. 170 (1) (1855) 59–86. doi:10.1002/andp.18551700105.

[53] J. George, N. V. Sastry, Densities, excess molar volumes, viscosities, speeds of sound, excess isentropic compressibilities, and relative permittivities for CmH2m+1(OCH2CH2)nOH (m = 1 or 2 or 4 and n = 1) + benzene, + toluene, + (o-, m-, and p-) xylenes, + ethylbenzene, and + cyclohexane, J. Chem. Eng. Data 48 (4) (2003) 977–989. doi:10.1021/je034005y.